Fibroblast to myofibroblast transition is enhanced by increased cell density

Mary T. Doolin[a], Ian M. Smith[a], and Kimberly M. Stroka[a,b,c,d,*]

[a]Fischell Department of Bioengineering and [b]Maryland Biophysics Program, University of Maryland, College Park, College Park, MD, 20742; [c]Center for Stem Cell Biology and Regenerative Medicine and [d]Marlene and Stewart Greenebaum Comprehensive Cancer Center, University of Maryland, Baltimore, Baltimore, MD, 21201

ABSTRACT **Idiopathic pulmonary fibrosis (IPF) is a chronic disease of the lung caused by a rampant inflammatory response that results in the deposition of excessive extracellular matrix (ECM). IPF patient lungs also develop fibroblastic foci that consist of activated fibroblasts and myofibroblasts. In concert with ECM deposition, the increased cell density within fibroblastic foci imposes confining forces on lung fibroblasts. In this work, we observed that increased cell density increases the incidence of the fibroblast-to-myofibroblast transition (FMT), but mechanical confinement imposed by micropillars has no effect on FMT incidence. We found that human lung fibroblasts (HLFs) express more α-SMA and deposit more collagen matrix, which are both characteristics of myofibroblasts, in response to TGF-β1 when cells are seeded at a high density compared with a medium or a low density. These results support the hypothesis that HLFs undergo FMT more readily in response to TGF-β1 when cells are densely packed, and this effect could be dependent on increased OB-cadherin expression. This work demonstrates that cell density is an important factor to consider when modelling IPF in vitro, and it may suggest decreasing cell density within fibroblastic foci as a strategy to reduce IPF burden.**

Monitoring Editor
Dennis Discher
University of Pennsylvania

Received: Aug 14, 2020
Revised: Oct 21, 2021
Accepted: Oct 25, 2021

INTRODUCTION

Idiopathic pulmonary fibrosis (IPF) is a chronic disease of the lung caused by a rampant inflammatory response that results in the deposition of excessive extracellular matrix (ECM). The excess ECM presents as scarring of the lung parenchyma and impairs gas exchange, making it difficult for patients to breathe (Martinez *et al.*, 2017). There are no effective treatments for IPF, and the median survival time after diagnosis is ~3 years, making IPF a critical disease to investigate and treat (Lan *et al.*, 2015).

Lung tissue explanted from patients diagnosed with IPF is stiffer than healthy lung tissue, due to the increased protein content of the ECM and altered collagen cross-linking (Burgstaller *et al.*, 2017; Jones *et al.*, 2018). Concomitant with increased ECM deposition and cross-linking, there is increased confinement imposed on cells by the ECM. In concert with increased confinement imposed by the ECM, there is increased confinement imposed by increased cell density as fibroblastic foci develop. These fibroblastic foci within the lung are another characteristic feature of IPF and consist of activated fibroblasts and myofibroblasts (Burgstaller *et al.*, 2017).

Myofibroblasts are contractile matrix-depositing cells characterized by α-smooth muscle actin (SMA)–positive stress fibers. Myofibroblasts are essential in the recovery of damaged tissues and critical in the inflammatory response, but cause pathology when they persist in tissue. Although the origin of myofibroblasts in IPF is continually under investigation, there is evidence that resident fibroblasts can differentiate into myofibroblasts, termed the fibroblast-to-myofibroblast transition (FMT), when given certain physical and/or chemical cues (Huang *et al.*, 2012). For example, fibroblasts cultured on stiff substrates are more likely to differentiate into myofibroblasts than those on soft substrates, due to increased actomyosin contractility (Huang *et al.*, 2012). Concomitantly, stiff matrices encourage stress fiber formation within cells, which compresses the nucleus (Swift *et al.*, 2013). However, it is unknown to what degree, if any, direct nuclear compression in the absence of increased contractility alters FMT. We are able to induce nuclear deformation within low-contractile cells by confining cells within the micropillar

This article was published online ahead of print in MBoC in Press (http://www.molbiolcell.org/cgi/doi/10.1091/mbc.E20-08-0536) on November 3, 2021.

*Address correspondence to: Kimberly M. Stroka (kstroka@umd.edu).

Abbreviations used: FMT, fibroblast-to-myofibroblast transition; HLF, human lung fibroblast; IPF, idiopathic pulmonary fibrosis.

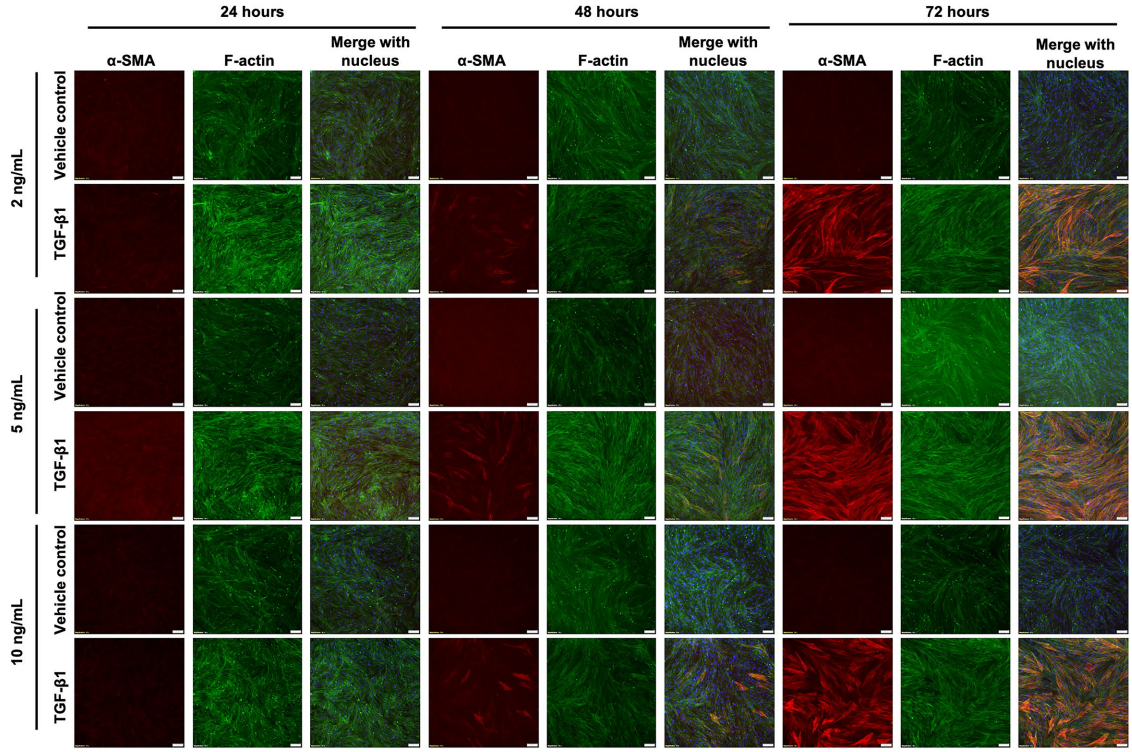

FIGURE 1: HLFs at high density increase α-SMA in response to TGF-β1, but this is time- and dose-dependent. HLFs were seeded at 12,000 cells/cm^2 and treated with 2, 5, or 10 ng/ml TGF-β1 or vehicle control for 24, 48, or 72 h. Cells were fixed and stained for α-SMA (red), f-actin (green), and the nucleus (blue). Scale bars represent 100 μm.

assay (Doolin and Stroka, 2019). This micropillar array also allows us to investigate whether increased confinement, such as that imposed by the dense ECM within IPF, influences FMT.

Confining forces can also come from neighboring cells within a tissue. In fibroblastic foci, fibroblasts and myofibroblasts are more densely packed than in healthy lung tissue. Cell density is known to affect the behavior of lung fibroblasts, such as how they contract a 3D collagen gel (Redden and Doolin, 2006). In this work, we investigated the role of mechanical and cell–cell imposed confinement in FMT. Our results enhance understanding of IPF progression at a mechanistic level and may potentially improve treatments for IPF.

RESULTS AND DISCUSSION

TGF-β1 incubation time alters α-SMA expression within human lung fibroblasts

TGF-β1 is a pro-inflammatory and pro-fibrotic cytokine that is upregulated in IPF (Fernandez and Eickelberg, 2012). TGF-β1 has been shown to induce FMT in vitro, as evidenced by increased α-SMA expression within HLFs (Kaarteenaho-Wiik *et al.*, 2009). Our first aim was to optimize the concentration and timing of TGF-β1 treatment to induce FMT by examining α-SMA expression via immunofluorescent straining. We observed α-SMA within HLFs after a 48-h incubation with TGF-β1 at 2, 5, or 10 ng/ml, and to a much greater extent after 72 h (Figures 1, 3). However, there was a decrease in the percentage of cells expressing α-SMA when we seeded HLFs at ~ 50% lower density (Figures 2, 3). At an even lower density, HLFs treated with 20 ng/ml TGF-β1 did not display the pronounced increase in α-SMA (Figure 4) that was observed in higher-density HLFs. With the potential cytotoxic effects of the citric acid carrier in mind, we chose 10 ng/ml TGF-β1 as our standard treatment concentration for subsequent experiments.

Human lung fibroblast seeding density alters myofibroblast-like expression within human lung fibroblasts

We next investigated if HLF response to TGF-β1 remained density-dependent beyond 72 h. We seeded 500, 5000, or 50,000 cells/cm^2 (low, medium, and high density, respectively) and treated with 10 ng/ml TGF-β1 for 5 d. We then examined α-SMA expression via immunofluorescent straining. We observed expression of α-SMA in HLFs seeded at medium or high density and treated with TGF-β1, but this effect was most prominent in HLFs seeded at high density (Figure 5A). Additionally, f-actin stress fibers were more prominent in medium and high-density groups. All groups treated with vehicle control and low-density cells treated with TGF-β1 were mostly devoid of α-SMA staining (Figure 5A). We confirmed these results via Western blot for the medium- and high-density groups, as the low-density group did not contain adequate protein for analysis (Figure 5, B and C). TGF-β1 induced much higher α-SMA protein expression in the high-density than in the medium-density group. However, the high-density group treated with vehicle control had higher levels of α-SMA than the medium-density vehicle control group by one order of magnitude. Consequently, TGF-β1 induced an ~14-fold increase in expression of α-SMA in the medium-density group and an ~21-fold increase in the high-density group. The increased α-SMA expression was present in both the cytosol and cytoskeleton portions of the HLFs (unpublished data). We also quantified nucleus area (Figure 5D) as a function of seeding density and treatment for the image sets represented in Figure 5A; these results will be discussed in more detail below.

The observation here that HLFs seeded at high density expressed more α-SMA in response to TGF-β1 than those seeded at low or medium density is in contrast to other results using fibroblasts sourced from different tissues. For example, one group showed that α-SMA expression increased when corneal fibroblasts were plated

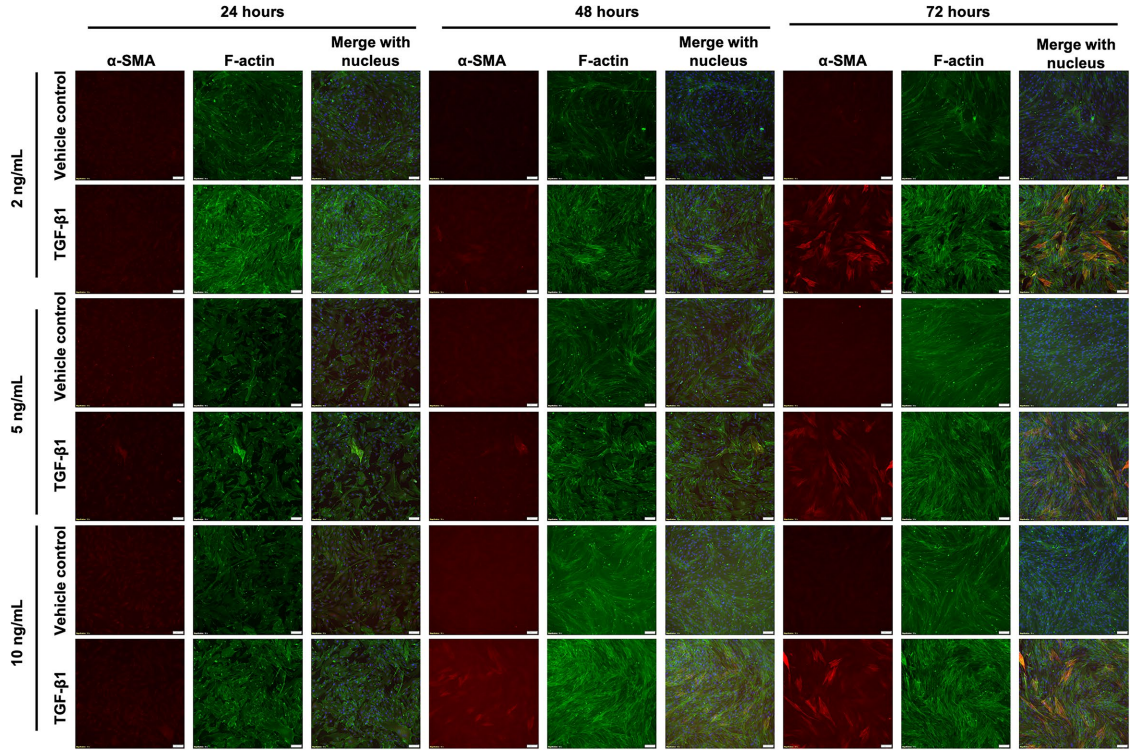

FIGURE 2: HLFs at medium density increase α-SMA in response to TGF-β1, but this is time- and dose-dependent. HLFs were seeded at 5000 cells/cm^2 and treated with 2, 5, or 10 ng/ml TGF-β1 or vehicle control for 24, 48, or 72 h. Cells were fixed and stained for α-SMA (red), f-actin (green), and the nucleus (blue). Scale bars represent 100 μm.

at low density (500 cells/cm^2) when compared with high density (50,000 cells/cm^2), even in the absence of TGF-β1 (Masur *et al.*, 1996). However, Masur *et al.* analyzed cells in each group once they reached confluence. Therefore, low-density cells were cultured for a longer time than high-density cells, on the order of days. This method for running the experiment could confound results, because substrate stiffness influences FMT, and traditional culture plastic is extremely stiff. Prolonged exposure to stiff plastic may induce FMT, and it has been shown that culture itself can induce FMT (Baranyi *et al.*, 2019). Others have demonstrated that medium-density bronchial fibroblasts (5000 cells/cm^2) undergo FMT more readily than high-density bronchial fibroblasts (50,000 cells/cm^2; Michalik *et al.*, 2011). However, this study investigated asthmatic bronchial fibroblasts, which is localized to a proximal site within the lung, while IPF affects distal alveoli. Again, Michalik *et al.* analyzed cells upon reaching confluence, with low-density cells cultured 8 d longer than high-density cells. Medium-density dermal fibroblasts undergo FMT more readily than high-density cells, potentially involving the upregulation of OB-cadherin (Ehrlich *et al.*, 2006).

Despite being FBS-deprived, HLFs were still able to proliferate at a very low rate. HLFs seeded at low and medium density doubled ~2–3 times in 6 d. HLFs seeded at high density doubled ~1–2 times in 6 d. This decrease in proliferation in the high-density group may be a confounding factor. For example, others have shown that quiescent myofibroblasts have reduced α-SMA turnover compared with proliferating cells (Arora and McCulloch, 1999). We assessed mitotic fraction of cells (Supplemental Figure S1) and nuclear Hoechst staining intensity (Supplemental Figure S2) in an effort to provide support that cells at high density may be quiescent; however, these data were inadequate to support this hypothesis.

It has been proposed that a transition within fibroblasts from N-cadherin expression to OB-cadherin expression is a hallmark of FMT (Pittet *et al.*, 2008). We seeded low-, medium-, and high-density HLFs and treated them with 10 ng/ml TGF-β1 for 5 d. We then performed a Western blot and noted that no group appeared to express N-cadherin (Figure 6A). Conversely, HLFs seeded at high density expressed more OB-cadherin than the medium-density group, and TGF-β1 treatment significantly increased OB-cadherin expression in the high-density group (Figure 6, B and C). HLFs seeded at low density showed very low OB-cadherin expression and thus were excluded from Figure 6C.

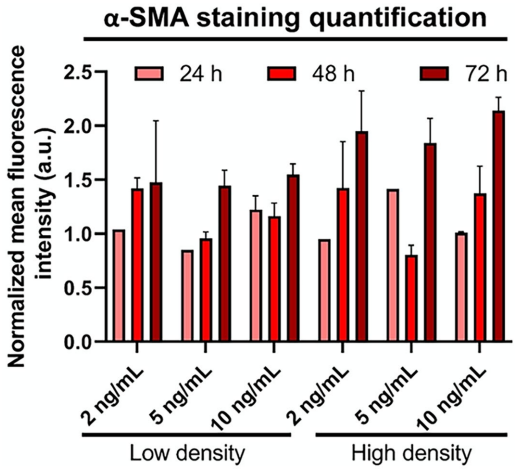

FIGURE 3: HLFs increase α-SMA in response to TGF-β1, but this is time- and density-dependent. Bars show mean fluorescence intensity across images for α-SMA for TGF-β1–treated group normalized to its respective control. Error bars represent standard error.

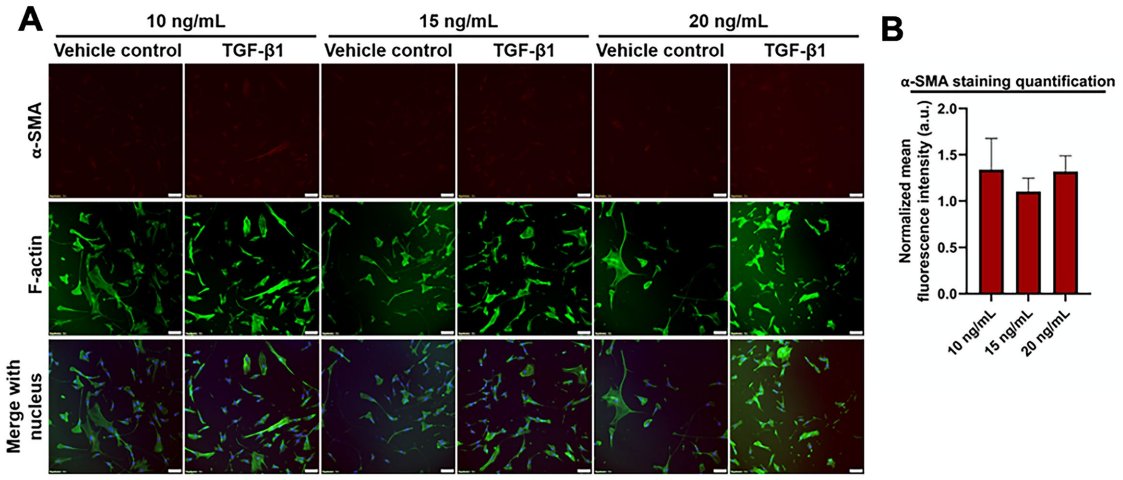

FIGURE 4: HLFs at low density do not increase α-SMA expression in response to TGF-β1. HLFs were seeded at 1000 cells/cm^2 treated with 10, 15, or 20 ng/ml TGF-β1, or vehicle control for 72 h. (A) Immunofluorescence images of cells were fixed and stained for α-SMA (red), f-actin (green), and the nucleus (blue). Scale bars represent 50 μm. (B) Bars show mean fluorescence intensity of α-SMA immunostaining for TGF-β1 treated group normalized to its respective control. Error bars represent standard error.

There is a shift from N-cadherin to OB-cadherin expression in fibroblasts during wound healing (Hinz *et al.*, 2004). Previously, blocking N-cadherin in bronchial fibroblasts was shown to reduce FMT (Michalik *et al.*, 2011). FOXF1 was recently demonstrated to be a key protein in preventing the switch from N-cadherin to OB-cadherin expression in FMT (Black *et al.*, 2018). Adherens junctions have been implicated in transferring mechanical strain between myofibroblasts, thereby opening mechanosensitive ion channels, inducing a calcium ion influx, and subsequently inducing contraction in the neighbor cell (Follonier *et al.*, 2008). Our results suggest

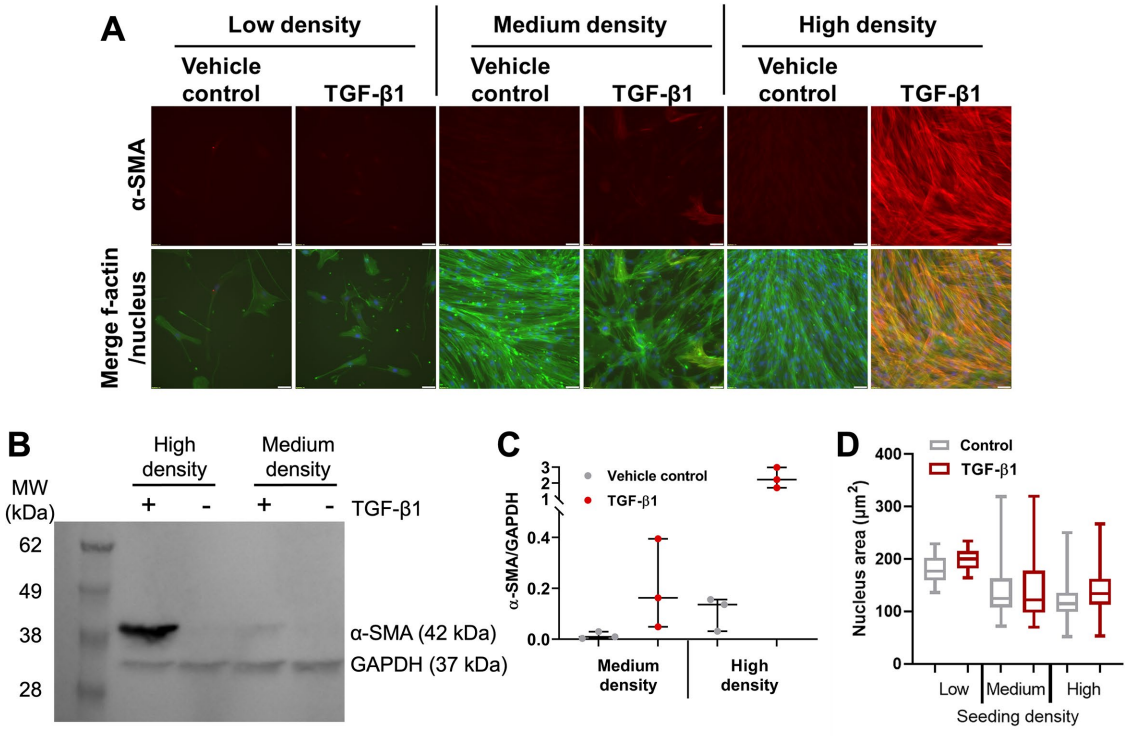

FIGURE 5: HLFs increase α-SMA expression with increasing cell density. HLFs were treated with 10 ng/ml TGF-β1 or vehicle control for 5 d. (A) Representative images of cells fixed and stained for α-SMA (red), f-actin (green), and the nucleus (blue). Scale bars represent 50 μm. (B) Representative Western blot. (C) Quantification of Western blots. Each dot in the dot plot represents one Western blot value and the center lines represent the median values. *$p = 0.0134$. (D) Box and whisker plots of quantified nuclear area for vehicle control and TGF-β1-treated HLFs at low, medium, and high seeding density, pooled from three independent experiments. Full statistical comparison tables for panel D are provided in Supplemental Table S1.

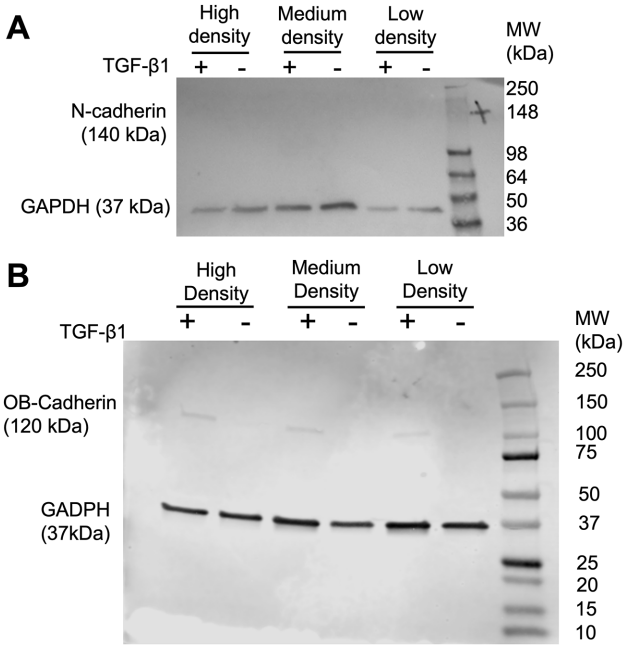

FIGURE 6: OB-cadherin expression is elevated in HLFs at high cell density. (A) Representative Western blot of N-cadherin. (B) Representative Western blot of OB-cadherin. (C) Quantification of OB-cadherin Western blots. Each dot in the dot plot represents one Western blot value and the center lines represent the median values. *$p<0.05$, **$p<0.01$, ***$p<0.001$.

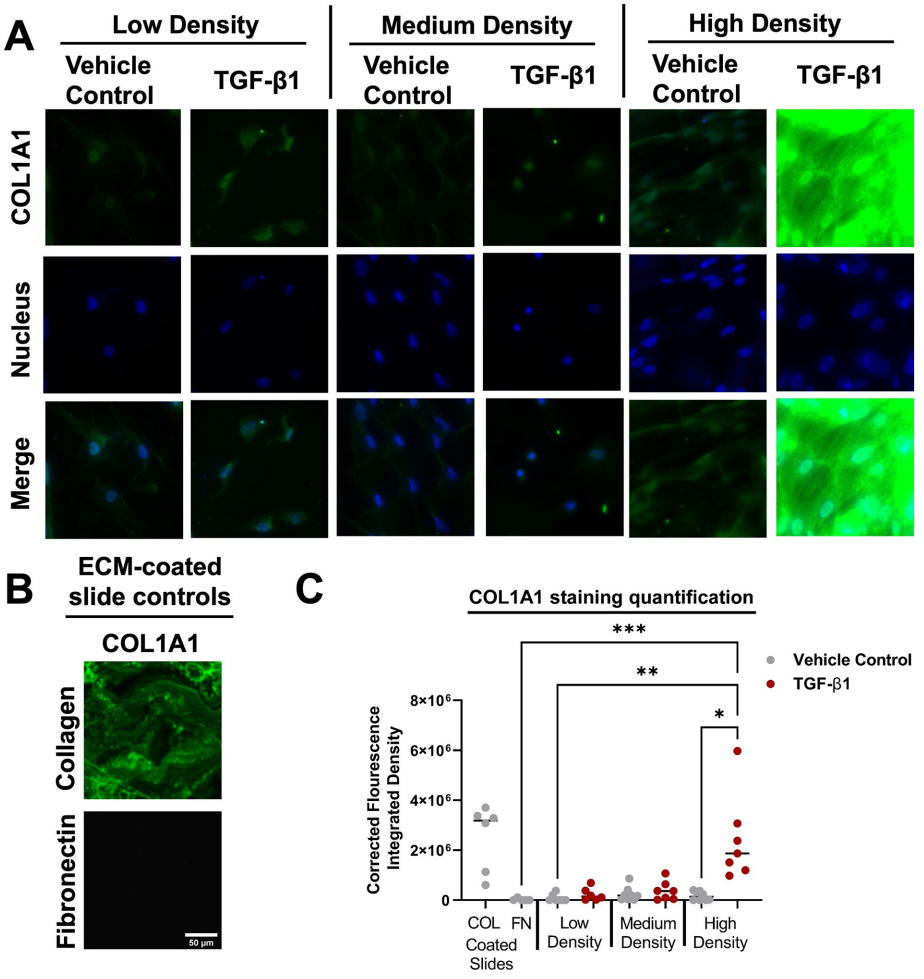

FIGURE 7: High-density HLFs deposit treated with TGF-β1 deposit more collagen matrix. (A) Representative immunostained images of COL1A1 (green) and the nucleus (blue). (B) Representative images of COL1A1 staining for collagen-coated and fibronectin-coated slides. Scale bar on fibronectin-coated slide image represents 10 μm and applies to all images in panels A and B. (C) Fluorescence integrated density values from immunostaining images. Each dot in the dot plot represents the mean value of one sample and the center lines represent the median values. *$p<0.05$, **$p<0.01$, ***$p<0.001$.

that increased HLF density up-regulates OB-cadherin, perhaps making cells more responsive to TGF-β1 due to their increased capacity for force transmission.

A combination of high seeding density and TGF-β1 promotes collagen matrix deposition

As mentioned above, it has been shown that myofibroblasts are matrix-depositing cells (Klingberg *et al.*, 2013). To assess the effects of seeding density on collagen matrix deposition, we seeded low-, medium-, and high-density HLFs onto fibronectin-coated glass slides and treated the cells with 10 ng/ml TGF-β1 for 5 d. Immunostaining of collagen type 1 motif alpha 1 (Col1A1) in these samples revealed that there is a dramatic increase in COL1A1 fluorescence for HLFs seeded at high density and treated with TGF-β1 (Figure 7A). Glass slides coated with collagen and with fibronectin were used as positive and negative controls, respectively (Figure 7B). Quantification of the immunofluorescence images supported our qualitative observations (Figure 7C). These results suggest that the combination of high-density seeding and TGF-β1 treatment is necessary to promote COL1A1 matrix deposition.

Cell confinement may not affect the fibroblast-to-myofibroblast transition

Cell density may impact cell behavior through physical deformation of the cell nucleus. As mentioned above, we quantified cell nucleus projected (2D) area from images (Figure 5A) of cells cultured at varying seeding densities. Cells (both control and TGF-β1 treated) seeded at medium and high density had significantly smaller nuclear areas than cells seeded at low density (Figure 5D; statistics in Supplemental Table S1). This led to the investigation of whether nuclear compression may influence FMT. Fibroblasts cultured on stiff substrates are more likely to

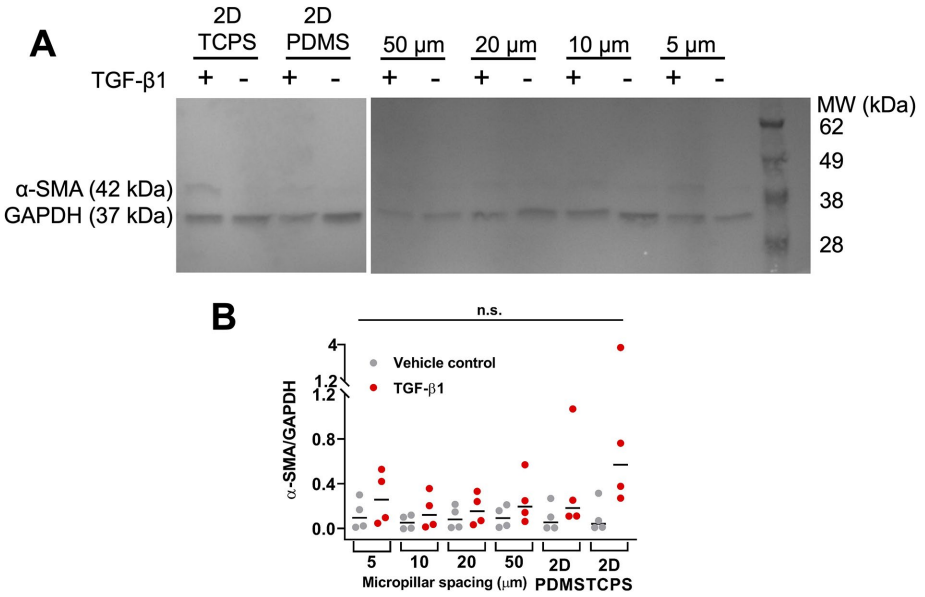

FIGURE 8: HLFs do not alter α-SMA expression with increasing confinement in a microfabricated micropillar system. (A) Representative Western blot. (B) Quantification of Western blots. Each dot in the dot plot represents one Western blot value and the center lines represent the median values. n.s. indicates not significant. TCPS: tissue culture polystyrene.

differentiate into myofibroblasts than those on soft substrates, due to increased actomyosin contractility and Yap/Taz signaling (Huang *et al.*, 2012; Liu *et al.*, 2015; Liang *et al.*, 2017). Concomitantly, stiff matrices encourage stress fiber formation within cells, and these stress fibers compress the nucleus (Swift *et al.*, 2013). However, it is unknown to what degree, if any, direct nuclear compression alters the FMT, in the absence of increased contractility.

To decouple the possible effects of increased actomyosin contractility and increased nuclear deformation on the observed density-dependent FMT, we used the micropillar assay previously developed in our laboratory to confine cells (Doolin and Stroka, 2019). We used PDMS micropillar arrays that are 5, 10, 20, or 50 μm apart from one another, as well as a 2D PDMS and 2D tissue culture polystyrene (TCPS) controls. This system allows nuclear deformation even in a reduced cell contractile state, that is, in the most confined micropillar array. TGF-β1 increased α-SMA expression at all levels of confinement by a small, though not statistically significant amount, with similar results on planar PDMS (Figure 8). Meanwhile, α-SMA expression was highest in HLFs treated with TGF-β1 on 2D TCPS. When we visualized cells via immunofluorescent staining, we noted that HLFs treated with TGF-β1 began to grow over the micropillar tops in the 5-μm group (Figure 9A). Additionally, HLFs treated with TGF-β1 tended to have higher f-actin signal and form discrete clumps, while control HLFs were more evenly distributed (Figure 9, A and B). It has been suggested that the formation of small contractile units is the most effective way to induce a high net force on a matrix (Tomasek *et al.*, 2002; Hinz *et al.*, 2004). It should also be noted that the addition of TGF-β1 can cause human lung fibroblasts to form gaps in their monolayer, as seen in the PDMS condition of Figure 9, likely due to enhanced cell contractility (Liu *et al.*, 2001; Epa *et al.*, 2015). An inhibitor of myosin II activity could reduce this artifact, but this treatment would also prevent FMT, and thus future work could focus on approaches for investigating the effects of modulating local cell density (Southern *et al.*, 2016; Sun *et al.*, 2021). Furthermore, our analysis of number of nuclei per image (Figure 9C; statistics in Supplemental Table S2) and mean nuclear area (Figure 9D; statistics in Supplemental Table S3) for cells in the micropillar devices suggested that there were no systematic differences in these values between micropillar spacings, which may have created confounding effects between cell density and confinement, especially when considering the seeding densities of our low-, medium-, and high-density conditions were 10-fold different from each other.

The above results indicate that there was no statistically significant effect of confinement on FMT within HLFs. Interestingly, our 2D PDMS control consistently had lower α-SMA expression than on 2D TCPS. We attribute this to several factors. PDMS is an innately hydrophobic material that we make hydrophilic via plasma treatment and then add a coating of collagen I. There is a possibility that collagen I attaches differently on plasma-treated PDMS vs TCPS. Additionally, there is the potential that PDMS may have adsorbed a portion of TGF-β1, a hydrophobic molecule, making it inaccessible to the cells. We addressed this by changing media every 1–2 d, but the potential for PDMS acting as a TGF-β1 sink should be investigated further. Additionally, the PDMS used here is ~ 1.75 MPa in stiffness, while TCPS is ~ 3 GPa (Johnston *et al.*, 2014). While both materials are extremely stiff, the three orders of magnitude increase in stiffness of TCPS could have induced a greater incidence of FMT.

Additionally, we note that the HLFs used in this study were isolated from a young, healthy female whose HLFs likely behave differently than those from an older or sick individual, because disease state has been shown to influence FMT. For example, bronchial fibroblasts derived from a patient with asthma underwent FMT with higher frequency than those from a non-asthmatic patient (Michalik *et al.*, 2011). Hence, we acknowledge that the age and health of HLF donors should be considered in interpreting and comparing results from different research groups.

IPF is a terminal disease with an average survival time of 3 years. There are no effective treatments for IPF, which highlights the urgent need for improved understanding of disease progression to elucidate new drug targets. Here we investigated how confining forces from neighboring cells or from physical features influence the lung FMT. In summary, we found that HLFs express more α-SMA in response to TGF-β1 when seeded at high density than at medium or low density. These results support the hypothesis that HLFs undergo FMT more readily in response to TGF-β1 when cells are densely packed. We speculate that this effect could be dependent on increased OB-cadherin expression. This work demonstrates that cell density is an important factor to consider when modeling IPF in vitro and may suggest decreasing cell density within fibroblastic foci as a strategy to reduce IPF burden.

MATERIALS AND METHODS

Request a protocol through *Bio-protocol*.

Cell culture

HLFs were authenticated by and purchased from ATCC (Manassass, VA, USA) and cultured in fibroblast basal medium (ATCC)

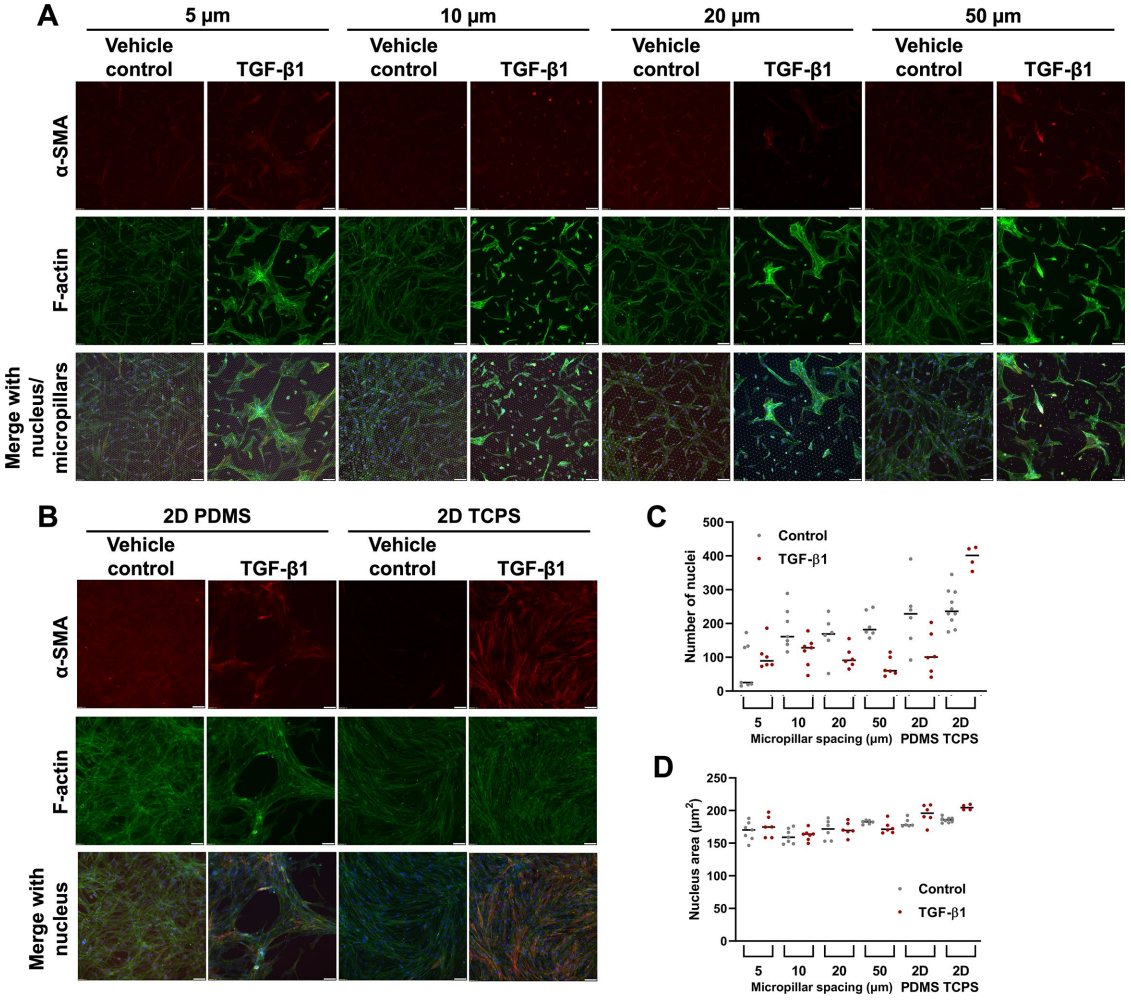

FIGURE 9: HLFs do not alter α-SMA expression with increasing confinement in a microfabricated micropillar system. Representative images of HLFs fixed and stained for α-SMA (red), f-actin (green), and the nucleus (blue), for cells (A) in microchannels or (B) on 2D PDMS or TCPS. Scale bars represent 50 µm. Also shown are dot plots for (C) mean number of nuclei per image and (D) mean nuclear area for conditions represented in images in panels A and B. Each dot in the dot plot represents the mean value of one image (data pooled from three independent experiments) and the center lines represent the median values. Full statistical comparison tables for panels C and D are provided in Supplemental Tables S2 and S3.

supplemented with 7.5 mM L-glutamine, 5 ng/ml FGF basic, 5 µg/ml insulin, 1 µg/ml hydrocortisone, 50 µg/ml ascorbic acid, 2% fetal bovine serum (FBS, ATCC), and 1% penicillin–streptomycin 10,000 U/ml (Thermo Fisher Scientific, Waltham, MA, USA). HLFs were cultured and used until passage 5. Cells were washed with phosphate-buffered saline (PBS; VWR, Radnor, PA, USA), detached with trypsin-EDTA for primary cells (ATCC), and resuspended in trypsin neutralizing solution (ATCC). All cells were cultured at 37°C and 50% humidity under 5% CO_2:95% air. Cells were checked for mycoplasma weekly by Hoechst staining and immunofluorescence microscopy.

Fibroblast-to-myofibroblast transition

To induce the FMT, HLFs were seeded and allowed to attach overnight. The following day, cells were washed with PBS before FBS-free media supplemented with 10 ng/ml TGF-β1 (Peprotech, Rocky Hill, NJ, USA) or vehicle control (10 mM citric acid) were added to induce FMT. For density-dependent experiments, cells were seeded at 500, 5000, and 50,000 cells/cm^2 for low, medium, and high densities, respectively, and media were changed every 1–2 d.

Micropillar array fabrication

Micropillar arrays were fabricated as previously described (Doolin and Stroka, 2019). Briefly, standard photolithographic techniques, as described previously, were used to create a silicon master of the micropillar array design, such that the pillars were 13–17 µm tall. All photolithography procedures were carried out in the University of Maryland Nanocenter FabLab. Polydimethylsiloxane (PDMS, Krayden, Denver, CO, USA) was mixed at a 10:1 base:curing agent ratio, poured over the silicon master, and baked to create a PDMS master, which was then removed and silanized overnight under vacuum using tridecafluoro-1,1,2,2,tetrahydrooctyl-1-trichlorosilane (OTS, 97%; UCT, Bristol, PA, USA). Then PDMS was mixed at a 10:1 base:curing agent ratio, poured onto the PDMS master, baked at 80°C overnight, and removed, yielding the final PDMS micropillar arrays. The micropillar arrays were placed in a plasma cleaner (Harrick Plasma, Ithaca, NY, USA) and plasma-treated with air for 2.5 min in order to increase hydrophilicity. PDMS blocks were simultaneously coated in 8% Pluronic F127 (Sigma-Aldrich) solution for 1 h at room temperature, and then washed with DI water. Micropillar arrays were subsequently stamped with the Pluronic F127-coated

PDMS blocks so that the pillar tops were rendered nonadhesive to cells and were placed in six-well plates. The micropillar-containing plates were UV sterilized for 10 min, and 20 μg/ml collagen I (Sigma-Aldrich) was added to all wells and incubated for at least 1 h at 37°C. The collagen I solution was then removed, and devices were washed with PBS before cells were seeded at a density of 5×10^4 cells/well. Cell media were changed every 1–2 d.

Immunofluorescence

The following steps were carried out at room temperature, unless otherwise specified. Cells were fixed in 3.7% formaldehyde (Fisher Scientific) for 10 min, and then washed twice in PBS (VWR). Cells were permeabilized with 0.5% Triton X-100 (Sigma-Aldrich) for 5 min, washed twice in PBS, and blocked for nonspecific binding in 2.5% goat serum (Abcam, Cambridge, MA, USA) for at least 1 h. Mouse anti-α-smooth muscle actin antibody (Sigma-Aldrich, St. Louis, MO, USA, #A5228, 1:100) in 1% goat serum was added to cells and incubated at 4°C overnight. Cells were washed three times in PBS, blocked in 2.5% goat serum for at least 1 h, and then incubated with AlexaFluor 488 Phalloidin (Thermo Fisher Scientific, 1:500), Hoechst (Thermo Fisher Scientific, 1:2500), and AlexaFluor 568 goat anti-mouse (ThermoFisher Scientific #A11004, 1:200) for 1 h. For collagen deposition experiments, mouse anti-Collagen 1A1 antibody (Santa Cruz Biotechnologies, Dallas, TX, USA, 3G3, 1:100) in 1% goat serum was added to cells and incubated at 4°C overnight. Cells were washed three times in PBS, blocked in 2.5% goat serum for at least 1 h, and then incubated with Hoechst and AlexaFluor 568 for 1 h. Cells were washed three times in PBS and then imaged. Images were acquired on an Olympus IX83 microscope (Olympus, Center Valley, PA, USA) using a 10×, 20×, or 60× magnification objective. The settings for each fluorescent channel were maintained across all images acquired within a given experiment. Image intensity can be compared within figures (and between Figures 1 and 2) but should not be directly compared across other figures, since they are from different experiments.

Cell lysis

Cells were washed with cold PBS, placed on ice, and then incubated for 5 min in ice-cold RIPA lysis buffer (Thermo Fisher Scientific) supplemented with 1:100 protease inhibitor cocktail (Sigma-Aldrich) and 1:500 10 mg/ml phenylmethylsulfonyl fluoride (PMSF) in ethanol. Cells were collected using a cell scraper, and samples were incubated on ice for 1 h, with vortexing every 15 min. Samples were centrifuged at $300 \times g$ for 6 min, and the cell lysate supernatant was collected. A Pierce BCA assay (Thermo Fisher Scientific) was performed to determine total protein concentration of each cell lysate against bovine serum albumin (BSA) standard.

Western blotting

Cell lysates were diluted in RIPA so that each sample was at the same concentration and final volume. Lysates were mixed 1:1 with 2× Laemmli sample buffer with 1:20 β-mercaptoethanol (BioRad, Hercules, CA, USA) and then incubated for 10 min at 100°C. Samples were loaded into precast 10% polyacrylamide gels (BioRad) and subjected to SDS–PAGE at 120 V for 1 h. Protein was then transferred to a polyvinylidene difluoride (PVDF) membrane (BioRad) at 100 V for 1 h. Membranes were blocked in Tris-buffered saline (TBS)-based blocking buffer (Thermo Fisher Scientific) for 1 h at room temperature and then incubated in primary antibody overnight at 4°C. Primary antibodies used include mouse anti-α-smooth muscle actin antibody (Sigma-Aldrich #A5228, 1:1000), rabbit anti-GAPDH (Cell Signaling Technology, Danvers, MA, USA, #2118, 1:2000), rabbit anti-OB-cadherin (Cell Signaling Technology #4442, 1:1000), rabbit anti-N-cadherin (Cell Signaling Technology #4061, 1:1000), rabbit anti-vimentin (Cell Signaling Technology #5741, 1:1000), and mouse anti-vimentin (Santa Cruz Biotechnology, Dallas, TX, USA, 1:2000). Membranes were then washed three times in TBS with 1:500 Tween 20 (TBST buffer, BioRad) at 4°C. Washed membranes were incubated in HRP linked secondary antibody for 1 h at room temperature. Secondary antibodies used were anti-mouse IgG (Cell Signaling Technology, #7076, 1:5000) and anti-rabbit IgG (Cell Signaling Technology, #7074, 1:5000). Membranes were then washed three times in TBST buffer and once in TBS buffer. Clarity Western ECL substrate was mixed with 1:1 peroxide solution:luminol/enhancer (BioRad) and then added to the membrane and incubated for 5 min. Membranes were imaged using a FluorChem E gel imaging system. Imaging was performed in the BioWorkshop core facility in the Fischell Department of Bioengineering at the University of Maryland, College Park.

Data analysis

Images of Western blot membranes were analyzed in ImageJ. Band intensity was measured within the same area for each lane. The *y*-axis on the plots shows the ratio of the protein of interest to GAPDH. A value of zero indicates that the protein is not expressed highly enough to be visualized via Western blot. Fluorescence images were quantified in ImageJ. Mean fluorescence intensity of each image was measured, and the TGF-β1 group was normalized to the vehicle control group. Fluorescence images were then adjusted in ImageJ for visualization. The brightness and contrast were adjusted in the same way for all images within a given fluorescent channel. For collagen staining, corrected fluorescence integrated density was determined by subtracting the background fluorescence from the total image fluorescence. Nuclear shape descriptions, including nucleus area, were determined using the analyze particles macro in ImageJ.

Statistical Analysis

Data from at least three independent trials was pooled for statistical analysis in all experiments. A Kruskal–Wallis test with Dunn's multiple comparisons test was performed. A significance level of $p = 0.05$ was used.

ACKNOWLEDGMENTS

This work was supported by a Burroughs Wellcome Career Award at the Scientific Interface (to K.M.S.), a University of Maryland Research and Scholarship Award (to K.M.S.), a Clark doctoral fellowship (to I.M.S.), the Fischell Department of Bioengineering, and the University of Maryland. Research reported in this publication was supported by the National Heart, Lung, and Blood Institute of the National Institutes of Health under Award F31HL145991 (to M.T.D.). The content is solely the responsibility of the authors and does not necessarily represent the official views of the National Institutes of Health. We acknowledge the support of the Maryland NanoCenter and its FabLab for providing photolithography resources. We acknowledge the BioWorkshop core facility in the Fischell Department of Bioengineering at the University of Maryland for plate reader and gel imager resources.

REFERENCES

Arora PD, McCulloch CAG (1999). The deletion of transforming growth factor-β-induced myofibroblasts depends on growth conditions and actin organization. Am J Pathol 155, 2087–2099.

Baranyi U, Winter B, Gugerell A, Hegedus B, Brostjan C, Laufer G, Messner B (2019). Primary human fibroblasts in culture switch to a myofibroblast-like phenotype independently of TGF beta. Cells 8, 721.

Black M, Milewski D, Le T, Ren X, Xu Y, Kalinichenko VV, Kalin TV (2018). FOXF1 inhibits pulmonary fibrosis by preventing CDH2–CDH11 cadherin switch in myofibroblasts. Cell Rep 23, 442–458.

Burgstaller G, Oehrle B, Gerckens M, White ES, Schiller HB, Eickelberg O (2017). The instructive extracellular matrix of the lung: basic composition and alterations in chronic lung disease. Eur Respir J 50, 1601805.

Doolin MT, Stroka KM (2019). Integration of mesenchymal stem cells into a novel micropillar confinement assay. Tissue Eng Part C Methods 25, 662–676.

Ehrlich HP, Allison GM, Leggett M (2006). The myofibroblast, cadherin, α smooth muscle actin and the collagen effect. Cell Biochem Funct 24, 63–70.

Epa AP, Thatcher TH, Pollock SJ, Wahl LA, Lyda E, Kottmann RM, Phipps RP, Sime PJ (2015). Normal human lung epithelial cells inhibit transforming growth factor-β induced myofibroblast differentiation via prostaglandin E2. PLoS One 10, 1–19.

Fernandez IE, Eickelberg O (2012). The impact of TGF-β on lung fibrosis: from targeting to biomarkers. Proc Am Thorac Soc 9, 111–116.

Follonier L, Schaub S, Meister JJ, Hinz B (2008). Myofibroblast communication is controlled by intercellular mechanical coupling. J Cell Sci 121, 3305–3316.

Hinz B, Pittet P, Smith-Clerc J, Chaponnier C, Meister J-J (2004). Myofibroblast development is characterized by specific cell–cell adherens junctions. Mol Biol Cell 15, 4310–4320.

Huang X, Yang N, Fiore VF, Barker TH, Sun Y, Morris SW, Ding Q, Thannickal VJ, Zhou Y (2012). Matrix stiffness-induced myofibroblast differentiation is mediated by intrinsic mechanotransduction. Am J Respir Cell Mol Biol 47, 340–348.

Johnston ID, McCluskey DK, Tan CKL, Tracey MC (2014). Mechanical characterization of bulk Sylgard 184 for microfluidics and microengineering. J Micromechan Microeng 24, 035017.

Jones MG, Andriotis OG, Roberts JJ, Lunn K, Tear VJ, Cao L, Ask K, Smart DE, Bonfanti A, Johnson P, *et al*. (2018). Nanoscale dysregulation of collagen structure-function disrupts mechano-homeostasis and mediates pulmonary fibrosis. Elife 7, 1–24.

Kaarteenaho-Wiik R, Pääkkö P, Sormunen R (2009). Ultrastructural features of lung fibroblast differentiation into myofibroblasts. Ultrastruct Pathol 33, 6–15.

Klingberg F, Hinz B, White ES (2013). The myofibroblast matrix: implications for tissue repair andfibrosis. J Pathol 229, 298–309.

Lan Y-W, Choo K-B, Chen C-M, Hung T-H, Chen Y-B, Hsieh C-H, Kuo H-P, Chong K-Y (2015). Hypoxia-preconditioned mesenchymal stem cells attenuate bleomycin-induced pulmonary fibrosis. Stem Cell Res Ther 6, 97.

Liang M, Yu M, Xia R, Song K, Wang J, Luo J, Chen G (2017). Yap /Taz deletion in Gli + Cell-Derived Myo fi broblasts attenuates fibrosis. 3278–3290.

Liu F, Lagares D, Choi KM, Stopfer L, Marinković A, Vrbanac V, Probst CK, Hiemer SE, Sisson TH, Horowitz JC, *et al*. (2015). Mechanosignaling through YAP and TAZ drives fibroblast activation and fibrosis. Am J Physiol - Lung Cell Mol Physiol 308, L344–L357.

Liu XD, Umino T, Ertl R, Veys T, Skold CM, Takigawa K, Romberger DJ, Spurzem JR, Zhu YK, Kohyama T, *et al*. (2001). Persistence of TGF-beta1 induction of increased fibroblast contractility. In Vitro Cell Dev Biol Anim 37, 193–201.

Martinez FJ, Collard HR, Pardo A, Raghu G, Richeldi L, Selman M, Swigris JJ, Taniguchi H, Wells AU (2017). Idiopathic pulmonary fibrosis. Nat Rev Dis Prim 3, 1–19.

Masur SK, Dewal HS, Dinh TT, Erenburg I, Petridou S (1996). Myofibroblasts differentiate from fibroblasts when plated at low density. Proc Natl Acad Sci USA 93, 4219–4223.

Michalik M, Pierzchalska M, Włodarczyk A, Wójcik KA, Czy J, Sanak M, Madeja Z (2011). Transition of asthmatic bronchial fibroblasts to myofibroblasts is inhibited by cell-cell contacts. Respir Med 105, 1467–1475.

Pittet P, Lee K, Kulik AJ, Meister JJ, Hinz B (2008). Fibrogenic fibroblasts increase intercellular adhesion strength by reinforcing individual OB-cadherin bonds. J Cell Sci 121, 877–886.

Redden RA, Doolin EJ (2006). Complementary roles of microtubules and microfilaments in the lung fibroblast-mediated contraction of collagen gels: dynamics and the influence of cell density. Vitr Cell Dev Biol - Anim 42, 70–74.

Southern BD, Grove LM, Rahaman SO, Abraham S, Scheraga RG, Niese KA, Sun H, Herzog EL, Liu F, Tschumperlin DJ, *et al*. (2016). Matrix-driven myosin II mediates the pro-fibrotic fibroblast phenotype. J Biol Chem 291, 6083–6095.

Sun X, Zhu M, Chen X, Jiang X (2021). MYH9 inhibition suppresses TGF-β1-stimulated lung fibroblast-to-myofibroblast differentiation. Front Pharmacol 11, 1–9.

Swift J, Ivanovska IL, Buxboim A, Harada T, Dingal PC, Pinter J, Pajerowski JD, Spinler KR, Shin JW, Tewari M, *et al*. (2013). Nuclear Lamin-A scales with tissue stiffness and enhances matrix-directed differentiation. Science (80-) 341, 965–966.

Tomasek JJ, Gabbiani G, Hinz B, Chaponnier C, Brown RA (2002). Myofibroblasts and mechano: regulation of connective tissue remodelling. Nat Rev Mol Cell Biol 3, 349–363.